Pulsating Solar Radio Emission*

A. Nindos[1] and H. Aurass[2]

[1] Section of Astrogeophysics, Physics Department, University of Ioannina, Ioannina GR-45110, Greece anindos@cc.uoi.gr
[2] Astrophysical Institute Potsdam, D-14482 Potsdam, Germany haurass@aip.de

Summary. A status report of current research on pulsating radio emission is given, based on working group discussions at the CESRA 2004 workshop. Quasi-periodic pulsations have been observed at all wavelength ranges of the radio band. Usually, they are associated with flare events; however since the late 90s, pulsations of the slowly-varying component of the Sun's radio emission have also been observed. Radio pulsations show a large variety in their periods, bandwidths, amplitudes, temporal and spatial signatures. Most of them have been attributed to MHD oscillations in coronal loops, while alternative interpretations consider intrinsic oscillations of a nonlinear regime of kinetic plasma instabilities or modulation of the electron acceleration. Combined radio spectroscopic observations with radio imaging and X-ray/EUV data have revived interest in the subject. We summarize recent progress in using radio pulsations as a powerful tool for coronal plasma and magnetic field diagnostics. Also the latest developments on the study of the physical processes leading to radio emission modulation are summarized.

1 Introduction

The interaction between the plasma and magnetic field produces several dynamic phenomena in the solar corona. Among them, significant attention has been paid to "pulsations" of the observed radiation. In the magnetized solar plasma, the eigenfrequencies of any oscillating system are determined by the magnetic field strength, and also the density and configuration of the magnetized plasma. Consequently, the determination of the oscillation properties helps us to derive information about the plasma and magnetic field parameters that is otherwise unavailable.

Over the years, several reports on temporal oscillations in the corona have been published. They cover almost all wavelengths with the majority in radio wavelengths (e.g. see the reviews by Aschwanden 1987; Aschwanden et al. 1999). The oscillations show a large variety in their periods, wavelengths, bandwidths, amplitudes, temporal and spatial signatures. This reflects the fact that pulsating emission can be generated by different physical mechanisms on different time and spatial scales. Most of

*Working Group Report

them have been attributed to MHD oscillations in coronal loops, while pulsations with irregular periodicities have been interpreted in terms of limit cycles of nonlinear wave-particle interactions in coronal loops. Another approach presumes a periodically repeated injection of nonthermal electrons into a coronal loop thus shifting the problem to a periodically acting accelerator.

Until the late 90s most reports on coronal pulsations came from time-series analysis of total flux temporal oscillations. With the development of suitable space-borne and ground-based instruments, the detection of spatially-resolved pulsations has become possible in EUV and microwave wavelengths. This led to the introduction of the term *coronal seismology*, even though the concept is not new: one compares the observed properties of the oscillations with theoretical modeling of the wave phenomena and obtains estimates of the coronal dissipative coefficients (e.g. Nakariakov et al. 1999) and magnetic field (e.g. Nakariakov and Ofman 2001). Usually, pulsating radio emission is associated with solar flares; however, since the late 90s, quasi-periodic oscillations of the slowly-varying component of the Sun's radio emission (i.e. emission from non-flaring active regions) have also been observed.

The radio domain is well known for its advantages, such as the possibility to observe the corona from the ground with unparalleled temporal resolution, the capability to probe the solar atmosphere from the chromosphere to the middle corona, the relative simplicity of (several) physical processes involved in the radio emission, the density resolution due to plasma emission, and the sensitivity to the magnetic field in the source volume. Of course, equally well known are its inherent limitations, for example the inferior spatial resolution and the influence of refraction effects and scattering. The above statements together with the prevalence of observations of radio pulsations in the literature justify the existence of the *Working Group on Radio Pulsations* at the CESRA Workshop on *The High Energy Solar Corona: Waves, Eruptions, Particles.*

In this report we attempt to capture the content of discussions held in the working group's sessions. In order to put the presentation of the issues on a concrete footing, in Section 2 we present a brief overview of radio pulsations. A detailed review of the subject appears in the article by Nakariakov and Stepanov in this volume. In Sections 3, 4, and 5 we present the issues discussed in the working group's sessions after we review –definitely not thoroughly– the existing literature. A summary and suggestions for future work are given in Section 6. Our report follows the traditional division into spectral ranges: microwave, decimetric and metric. This is certainly arbitrary in terms of the underlying physics responsible for the radio events but it is justified mainly by the fact that a self-consistent picture covering all aspects of radio pulsations in the solar corona is still missing. Although our working group did not solve any problems, we believe that we did make some progress in putting together some of the observational data and pointing out outstanding questions.

2 A Brief Overview of Radio Pulsations

2.1 Pulsations Associated with Transient Activity

Quasi-periodic pulsations of coronal radio emission have been observed extensively for many years. In solar radio astronomy, the term "pulsation" sometimes is used liberally to describe single-frequency total flux time profiles showing repeated ups

and downs quasi-periodically. For early examples, the reader is refered to Elgarøy (1977), who reported continuum fluctuations of noise storms and type IV bursts with minute time-scale, and Dröge (1971) who first described decimetric pulsations. This definition does not tell anything about the spectral bandwidth of the fluctuations and may contribute to significant ambiguity in the interpretation of observations. For example, groups of type III bursts, type II burst herring-bone fine structures, and so called broad-band pulsations can all appear as quasi-periodic oscillations on single frequency records despite the fact that they reflect completely different physical processes.

Consequently, additional spectral information is needed when studying periodic fluctuations of the total radio flux at discrete frequencies. The first spectral data showing metric broad band pulsations were presented by Young et al. (1961). For decades, radio spectra were recorded on film. Now the digital recording and processing of broad band receiver data gives much easier access to the data, especially to fast intensity fluctuations with time and frequency.

Radio pulsations have been observed at all wavelength ranges of the radio band: metric, decimetric and microwaves. They demonstrate a rich diversity of observational features. Periods from 10^{-2} to 10^{3} s have been reported. The pulse amplitude and pulse periodicity range from almost constant to rapidly varying. Broad-band (e.g. $\Delta f/f \approx 1$) and narrow-band (e.g. $\Delta f/f \leq 0.1$) pulsations have been detected.

Typical examples of radio pulsations are given in the dynamic spectra of Figure 1 (narrow-band pulsations in Figure 1b and broad-band pulsations in Figure 1a). Broad-band pulsating structures are a well-known fine structure phenomenon appearing in dynamic spectra of solar type IV continuum emission. Their characteristic period is of the order of 1 s (e.g. Abrami 1970, McLean and Sheridan 1973, Slottje 1981). Pulsating sources were first imaged with the Japanese 160 MHz interferometer (Kai and Takayanagi, 1973), and later with the French Nançay Radio Heliograph (NRH), see Trottet et al. (1981). Also a variety of other patterns can be superposed on metric and/or decimetric continua: intermediate drift or fiber bursts, with bandwidths below 10 MHz, durations of less than 1 s and drift rates between the fast (type III) and slow (type II) drift bursts. Furthermore, zebra patterns of almost parallel, drifting emission bands and spike bursts can occur as superposed continuum fine structures.

Fiber bursts, spikes, and zebra patterns do not belong to periodic pulsations in the strict sense of the term. But sometimes all these phenomena cannot be distinguished easily for two reasons: first, they cannot be discriminated with single frequency records alone, and second, all these fine structures can occur, at least in the metric range, in continuum patches together (with the term "continuum patches" we mean structures with duration too long for a type III burst and too short for a type IV burst), sometimes seemingly in a systematic sequence in time. Therefore a common source mechanism has been invoked (e.g. Kuijpers 1980). Because of this situation, we did not exclude the above-mentioned fine structure phenomena from the present article about pulsating radio phenomena.

The pulsating radio emission can come from either a coherent or incoherent emission mechanism. When the pulsations show narrow spectral bandwidth, a coherent mechanism should be involved. The physical mechanisms producing quasi-periodic pulsations have been grouped into three categories e.g. by Kuijpers (1980) and Aschwanden (1987).

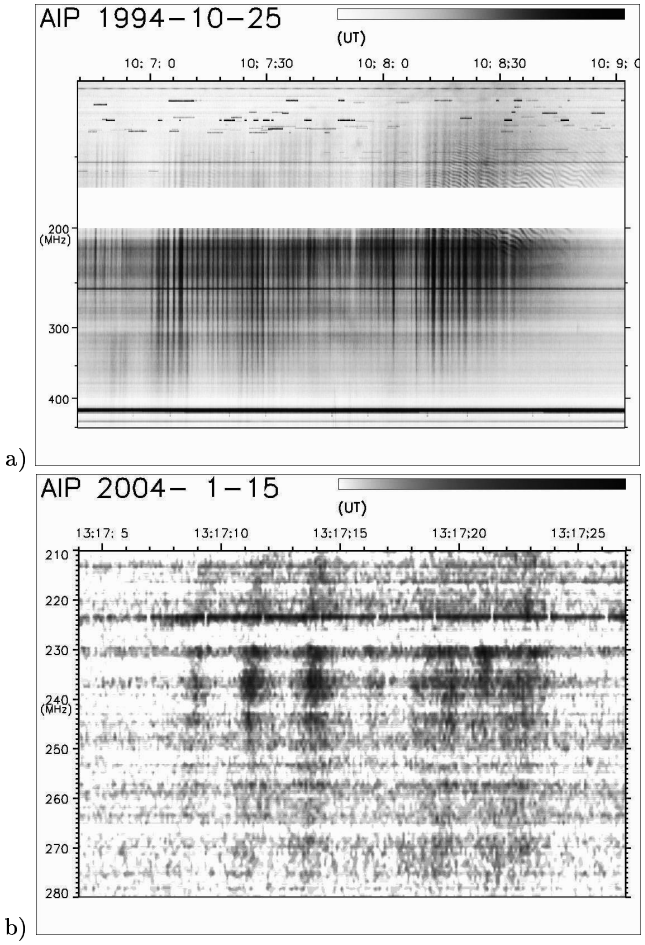

Fig. 1. Examples of meter-wave pulsations. a) Event of October 25, 1994, complex type II/IV burst (Aurass et al. 2003). Broad-band pulsations with more than 100 single pulses, followed–at the low frequency edge–by more than 20 parallel zebra stripes. The zebra stripes are sometimes already visible between the pulsation pulses. The low frequency limit in Figure 1a is 110 MHz. b) Event of January 15, 2004. Faint isolated narrow-band pulsation event of 5 pulses only, but with the same period as in a). Their comparison with Trieste single frequency records confirmed their solar origin (courtesy J. Magdalenić).

1) MHD oscillations of a magnetic loop which modulate the radio emission. There are three branches of solutions of the dispersion relation for propagating and standing MHD waves: the slow-mode branch (with acoustic phase speed) and the fast-mode and Alfvén branch (both with Alfvénic phase speed). Each branch has a symmetric and asymmetric solution, named the sausage and kink modes (Roberts et al. 1984). The fast kink mode produces a lateral translation of the

loop but does not modify magnetic field strength or particle density. Consequently, it is difficult to modulate radio emission with the kink mode. The longitudinal (slow magnetoacoustic) mode yields periods much longer than the ones usually observed in radio. Numerous nonimaging radio observations with periods of about 0.5 s up to some minutes have been interpreted in terms of the fast sausage mode. Ideally, it is a mode in which a slender flux tube oscillates via standing symmetric fast mode waves (Roberts et al. 1983). Fast mode waves can propagate only if the Alfvén speed in the loop is slower than in the surroundings; i.e. the loop must be overdense. If we assume a cylindrical symmetry, the period is determined by the length of the loop (e.g. Nakariakov et al. 2003).

The generation of MHD oscillations is usually associated with either the initial energy release in the dense kernel of the flare (Zaitsev and Stepanov 1982), or with plasma flows induced by chromospheric evaporation (Zaitsev and Stepanov 1989). Alternative mechanisms are the particle acceleration in current sheets (Aschwanden 1987) and in colliding current-carrying loops (Sakai and de Jager 1996), and in a single current-carrying loop considered as an LCR-circuit (Zaitsev et al. 1998).

2) Intrinsic oscillations of the flux created by an oscillatory nonlinear regime of the kinetic plasma instabilities that emit the radio waves. Oscillatory wave-wave interactions (e.g. Zaitsev 1971) and wave-particle interactions (e.g. Stepanov 1980) have been considered. The common ingredient of these mechanisms is that the pulsating regime corresponds to the limit cycle in phase space of a nonlinear dissipative system, and thus may show smaller (for linear disturbances) or larger (for highly nonlinear conditions) deviations from strict periodicity.

3) **Modulation of acceleration.** Here, one idea is that the pulsating radio emission comes from a resonant region which is driven by external dynamics. An example is the model by Kliem et al. (2000) which has been used for the interpretation of some decimetric pulsations: the model invokes quasi-periodic particle acceleration episodes that result from a dynamical regime of magnetic reconnection in a large-scale current sheet. This process leads to the formation of a growing plasmoid, which becomes strongly accelerated along the sheet, and to a pulsating particle source at the magnetic X line adjacent to the plasmoid. Alternatively, referring to the analysis of X-ray and microwave observations by Hanaoka (1996), the interaction between a small-scale emerging loop hosting the particle accelerator, and a large-scale loop being a trap for injected particles and containing the pulsating radio source, has been considered. Such an approach sometimes helps us understand the excitation of meter-wave pulsations (Zaitsev et al. 2005).

2.2 Quasi-Periodic Oscillations of the Microwave Slowly-varying Component

The fact that the atmosphere above sunspots shows modes of oscillatory behavior, visible as intensity and velocity variations, is well known for several decades (e.g. see the reviews by Lites 1992, and Staude 1999). In the umbral photosphere, oscillations with periods in the five–minute range as well as in the three–minute range occur. At chromospheric levels the intensity and velocity oscillations with periods of 150–200 s show larger amplitudes and are observed in the inner part of the umbra. Reports of photospheric magnetic field oscillations also exist (e.g. Ruedi et al. 1998; Norton et al. 1999). However, it seems that, at least in some of the reported observations of

photospheric magnetic field oscillations, instrumental effects have an important contribution to the observed oscillatory pattern (e.g. Bellot-Rubio et al. 2000). Observations with instruments on board SOHO (Solar and Heliospheric Observatory) have confirmed the presence of mostly 3-minute oscillations in the coronal-chromosphere transition region (TR) above sunspots (e.g. Fludra 1999; Brynildsen et al. 1999a). Usually, they affect the entire umbral TR and part of the penumbral TR. Most of them are compatible with the hypothesis that the oscillations are caused by linear, upward–propagating progressive acoustic waves (however, Brynildsen et al. 1999b reported nonlinear oscillations in the TR of one sunspot).

Since the late 90s, in addition to the microwave pulsations associated with flare activity, quasi-periodic oscillations of the slowly varying component of the microwave emission of active regions have been detected (Gelfreikh et al. 1999; see also Gopalswamy et al. 1993). These pulsations are observed primarily above sunspots and, in principle, are independent of any flare activity. The sunspots involved emit strong stable gyroresonance radiation. Gelfreikh et al. (1999) used Nobeyama Radioheliograph (NoRH) data at 17 GHz and measured the circular polarization (V) flux of several such sources as a function of time; they detected nearly harmonic oscillations with periods mostly between 120–220 s.

In order to discuss the origin of these oscillations we briefly remind the reader of the properties of the gyroresonance emission mechanism (for more details see, e.g., the review by White and Kundu 1997). Gyroresonance is a resonant mechanism: opacity is significant only in thin layers where the observing frequency is a low–integer multiple of the local gyrofrequency. The gyroresonance emission in the extraordinary (x) mode comes primarily from the third or lower harmonics of the gyrofrequency, whereas ordinary (o) mode emission has less opacity and comes from the second harmonic. The structure of the source depends upon which of the low–order (second to third; the fourth may play some role in big sunspots very close to the limb) harmonics of the gyrofrequency are located in regions of high temperature. This, in turn, depends on the frequency and the magnetic field. The brightness temperature of a harmonic that satisfies the above condition is determined by the electron temperature at the height where it is located and by its opacity. The opacity has much stronger dependence on the angle θ between the magnetic field and the line of sight than on any other physical parameter such as temperature and density. Gelfreikh et al. (1999) interpreted the periodic fluctuations of the V flux they detected in terms of MHD oscillations which result in variations of the size of the emitting gyroresonance layer and its temperature.

Furthermore, Shibasaki (2001) detected 3–min oscillations in the 17 GHz emission of a sunspot for which 3–min velocity and intensity oscillations due to upward–travelling acoustic waves had been detected in TR lines observed by SUMER. Shibasaki (2001) applied the values of density and temperature fluctuations deduced from SUMER to the sunspot's gyroresonance emision and found good agreement with the detected radio oscillation. He attributed the 3–min oscillation to the resonant excitation of the cut–off frequency mode of the temperature plateau around the temperature minimum. Using the VLA at 8.5 and 5 GHz, Nindos et al. (2002) were able to detect spatially resolved oscillations in both the total intensity and circular polarization emission of a sunspot-associated gyroresonance source (see Section 3.2 for more details).

3 Microwave pulsations

3.1 Flare-related Microwave Pulsations

Microwave bursts often display quasi-periodic pulsations with periods from about 40 msec in narrow-band bursts (e.g. Fleishman et al. 2002) up to 20 sec in broad-band bursts (e.g. Nakajima 1983; Stepanov et al. 1992; Qin et al. 1996; Asai et al. 2001; Grechnev et al. 2003). While the narrow-band bursts require a coherent mechanism to be involved, the broad-band bursts are generated by the gyrosynchrotron emission mechanism which is very sensitive to the magnetic field in the radio source. Broad-band microwave flux pulsations with periods $P \approx 1 - 20$ s are believed to represent some kind of magnetic oscillations that modulate the efficiency of gyrosynchrotron radiation or electron acceleration itself (see Section 2.1).

Fleishman (see also Fleishman et al. 2002) presented two events showing periodic narrow-band millisecond pulsations of the microwave emission both in total intensity and circular polarization. He found unusually large delays between the right and left-hand circularly polarized radiation, and showed that the radio emission was generated as unpolarized by a plasma mechanism at the second harmonic of the upper-hybrid frequency. His analysis demonstrated that the observed oscillations of the degree of circular polarization could be understood in terms of a group delay between x-mode and o-mode along the line of sight. The predicted theoretical dependence of the group delay with frequency ($\propto f^{-3}$) agreed very well with the observed frequency dependence of the delay between the right-handed and left-handed polarized components of oscillations. Also the authors were able to deduce a number of source parameters in addition to the density and magnetic field strength of the background plasma.

Fleishman also presented a theoretical study which shows that the mechanism of transition radiation (i.e. radiation generated by charged particles as they move through a boundary between two media having different dielectric permeabilities, or when they move through a spatially or temporally inhomogeneous medium) in turbulent dense media (Platonov & Fleishman 2002) yields common microwave and decimetric sources out of the same loop structure and from the same energetic particle ensemble. This is interesting because it provides a link to emission features frequently occurring at both spectral ranges.

Sheiner reported microwave pulsations before strong flares. She derived periods of 5-6 s for pulsations at $\lambda = 3$ cm and periods of 7-9 s at $\lambda = 10$ cm. Careful follow-up is needed in order to check whether instrumental effects do not contribute to the reported oscillatory patterns.

Reznikova and Melnikov reported spatially resolved oscillations in a flaring loop observed at 17 and 34 GHz with NoRH (see also Nakariakov et al. 2003; Aschwanden et al. 2004). The total flux integrated over the entire source did not reveal oscillations; the oscillations were apparent at selected $10'' \times 10''$ regions at the footpoints and loop top of the flaring loop (see Figure 2). The oscillations were interpreted in terms of sausage magnetoacoustic modes. First, they showed that the oscillation period of the global sausage mode is determined by the loop length and the density contrast between the loop and its environment. They noted that the previously used expression for the sausage-mode oscillating period (depending primarily on the ratio of the loop cross-section radius and the Alfvén speed inside the loop) is not correct

because it does not take into account the highly dispersive nature of the phase speed and the long-wavelength cutoff of the wavenumber.

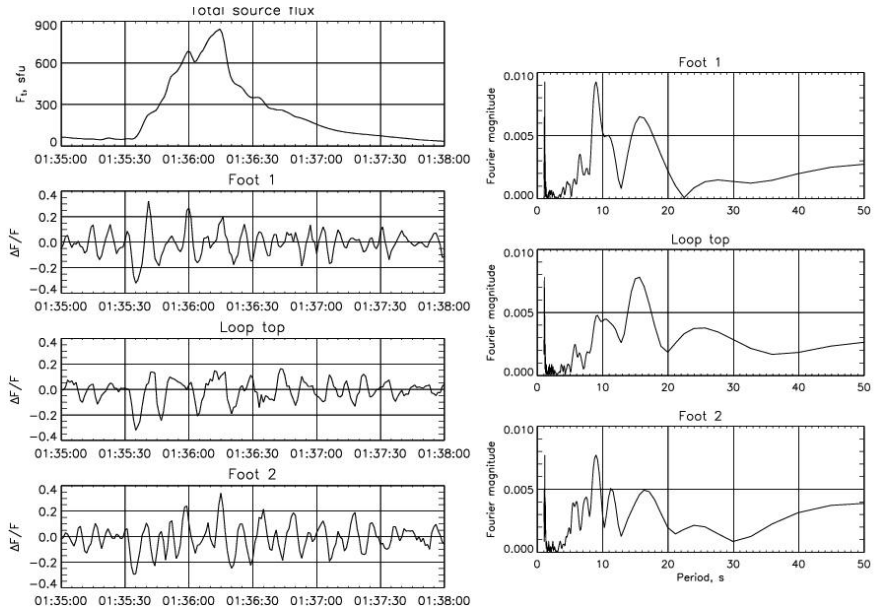

Fig. 2. NoRH observations of the 2000 January 12 flare at 17 GHz. The left column shows the time profiles and the right column shows the corresponding power spectra. The top left panel refers to the entire flaring loop while the other panels refer to the footpoints and loop top (from Nakariakov et al. 2003).

The analysis of their observations showed that the 17 and 34 GHz emissions exhibited synchronous quasi-periodical variations of the intensity at the loop top and footpoints of the flaring loop. Detailed comparison of the derived power spectra showed that the pulsations at the footpoints were almost synchronous with period of P_2 = 8-11 s. At the loop-top, the synchronism with the footpoint pulsations was not so prominent but nevertheless it existed on larger time scales of P_1 = 14-17 s. Reznikova and Melnikov pointed out that these properties of the pulsations indicate the possibility of simultaneous existence of two modes of sausage oscillations in the loop: the global mode with period of P_1 = 14-17 s and the nodes at the footpoints, and the harmonic with P_2 = 8-11 s.

3.2 Quasi-periodic Oscillations of the Slowly-varying Component

Using VLA data, Nindos (see also Nindos et al. 2002) presented the first spatially resolved oscillations in total intensity and circular polarization of a stable

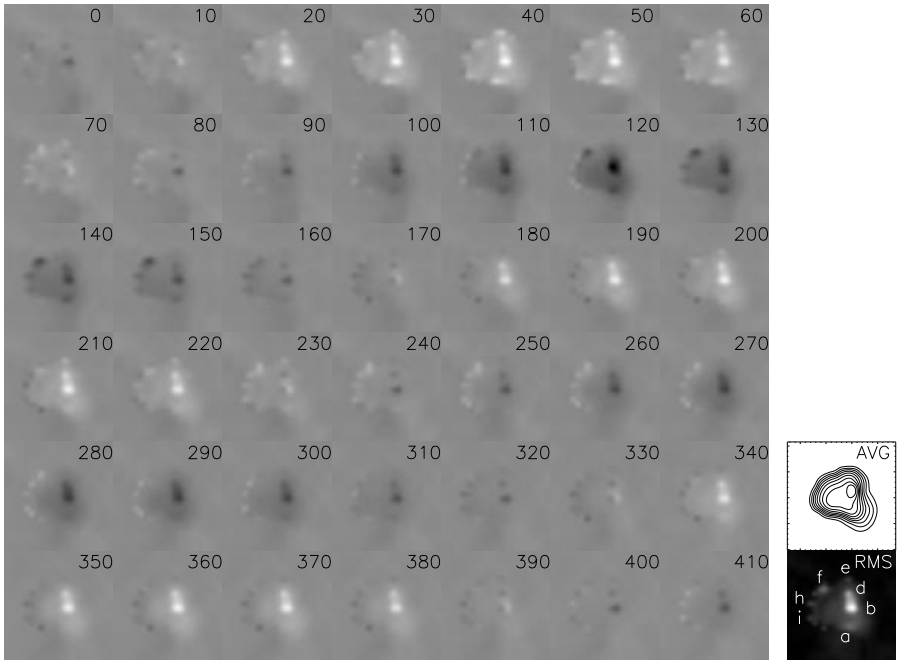

Fig. 3. 8.5 GHz I snapshot difference images obtained every 10 s between 22:19:00–22:26:00 UT. In the rightmost column the average and rms images derived from the entire 22:19:00–22:32:20 UT time series are presented. The difference images were produced after subtracting the average image from each snapshot image. White represents positive flux and black represents negative flux (from Nindos et al. 2002).

sunspot-associated gyroresonance source. Intermittent oscillations with, nevertheless, remarkable positional, amplitude, and phase stability were detected at 8.5 and 5 GHz. The spatial distribution of intensity variations was patchy and the location of the patches of strong oscillatory power was not the same at both frequencies. The strongest oscillations were associated with a small region where the 8.5 GHz emission came from the second harmonic of the gyrofrequency (see Figure 3) while distinct peaks of weaker oscillatory power appeared close to the outer boundaries of the 8.5 and 5 GHz gyroresonance sources, where the emissions came from the third harmonic of the gyrofrequency. At both frequencies the oscillations had periods in the three–minute range: the power spectra showed two prominent peaks at 6.25–6.45 mHz and 4.49–5.47 mHz.

The authors checked the observed properties of the oscillations against model computations of the gyroresonance emission. They found that the oscillations are caused by variations of the location of the third and/or second harmonic surfaces with respect to the base of the TR, i.e. either the magnetic field strength or/and the height of the base of the TR oscillates. The best–fit model to the observed microwave oscillations can be derived from photospheric magnetic field strength

oscillations with an rms amplitude of 40 G or oscillations of the height of the base of the TR with an rms amplitude of 25 km. Furthermore small variations of the orientation of the magnetic field vector yielded radio oscillations consistent with the observed oscillations.

Gelfreikh reported quasi-periodic microwave oscillations of several types of stable sources. The oscillations were detected using a variety of instruments: the RATAN-600, NoRH, the Siberian Solar Radio Telescope (SSRT) and the Crimean RT-22. The most prominent oscillations were associated with sunspots showing periods of about 3 minutes. In some sunspots, however, oscillations with shorter and longer (up to 180 minutes) periods were detected. He detected oscillations not only above suspots but also above plages and pores. He pointed out the interesting result that sometimes within the same active region, different areas oscillate with different periods. Usually the plage-associated oscillations exhibited periods of about 10 minutes, but longer periods of about 50-80 minutes were not rare. He discussed possible mechanisms responsible for the observed oscillations and showed that acoustic modes with periods less than 1 min strongly dissipate in the lower solar corona due to thermal conduction losses while oscillations with periods of 10-40 s are associated with Alfvén disturbances.

4 Decimetric Pulsating Emission

4.1 Broad-band Pulsations

The decimetric pulsations are broadband emissions ($\Delta f/f$ about 0.5) with periodic or irregular short fluctuations. Sometimes they are quasi-periodic with pulses of 0.1 to 1 s separations, occurring in groups of some tens to hundreds and lasting a few seconds to minutes. As in the meter-wave range, the morphology shows considerable differences in modulation depths. Some decimetric events occur in continuum patches with drifting upper and lower frequency boundaries, with the drift being predominantly directed toward lower frequencies. Such patches are called drifting pulsating structures (DPS).

Traditionally, the emission of decimetric pulsations has been interpreted by a loss-cone instability of trapped electrons (Kuijpers 1980, Aschwanden & Benz 1988). An alternative interpretation of a decimetric drifting pulsating event (see Figure 4) was presented by M. Karlický. This flare shows drifting pulsating structures of varying bandwidth in the 0.8-2 GHz range before the hard X-ray peak. In the main hard X-ray phase, the radio intensity increases and pulsations become less regular. *Yohkoh* soft X-ray images of this flare (Ohyama and Shibata 1998) revealed a nearly stationary low-lying flare loop and a plasmoid ejection, which was firstly seen at 9:24:40 UT at a height of $\approx 2 \times 10^4$ km. The ejected plasmoid was continuously accelerated up to a speed of $\approx$250 km s^{-1} at 09:25 and $\approx$500 km s^{-1} at 09:26 UT. The drifting pulsating structures of this event are interpreted in the framework of a model in which the radio pulsations are caused by quasi-periodic particle acceleration episodes that result from magnetic reconnection in a large-scale current sheet (Kliem et al. 2000). Under these circumstances, a possible reconnection model is the one that reconnection is dominated by repeated formation and subsequent coalescence of magnetic islands. This process is known as secondary tearing or impulsive bursty regime of reconnection. The continuously growing plasmoid is fed by newly

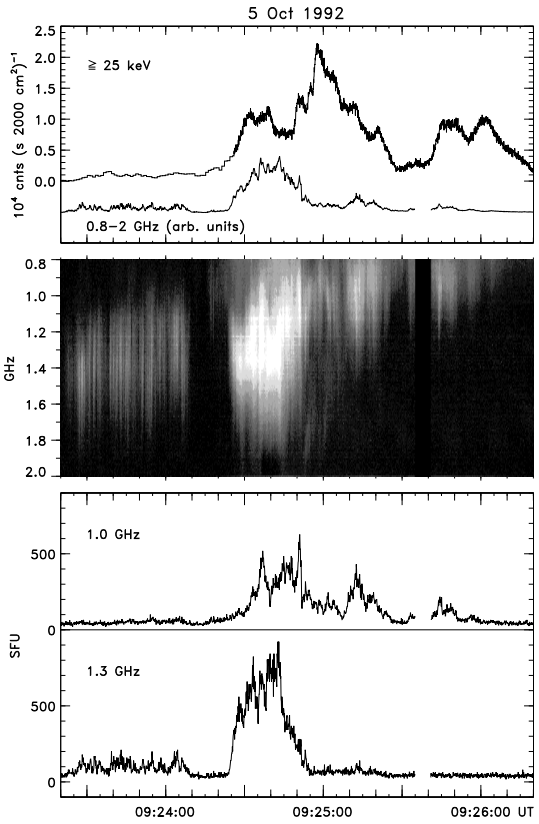

Fig. 4. Event of October 5, 1992 (from Kliem et al. 2000). Dynamic radio spectrum (Ondřejov) (middle), two single-frequency cuts of the spectrum (bottom), and CGRO/BATSE/DISCSC hard X-ray light curve (top).

coalescing islands. The plasmoid becomes strongly accelerated along the sheet and the pulsating particle source is located at the magnetic X line adjacent to the plasmoid. The radio source is then formed in or near the plasmoid. The frequency drift of the pulsating structures can naturally be attributed to the rise of the plasmoid in the corona, or to the growing upward expansion of the current sheet.

Other studies (Hori 1999; Khan et al. 2002; Karlický et al. 2002; Karlický 2004) found drifting pulsating structures to be associated with the impulsive phase of flares, although they can occur before or after the HXR burst peak, and can be associated with plasma ejections seen in soft X-rays or EUV. At the workshop, Karlický presented one example of drifting pulsating structures observed during the X1.5 flare of March 18, 2003. The DPS was associated with a moving X-ray source mapped by RHESSI's 12-25 keV channel. Karlický presented a cartoon model which is shown in Figure 5 attributing the different sources of DPS indicated by patch se-

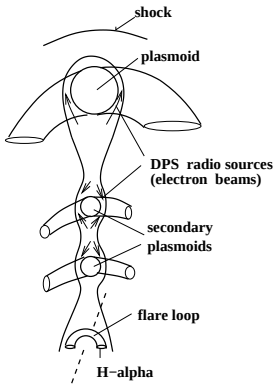

Fig. 5. Multiple decimetric pulsating source model as proposed by Karlický (2004) giving an idea about a possible current sheet evolution in the main flare phase.

quences observed in some decimetric dynamic spectra to the possible fragmentation of the evolving flare current sheet.

Khan showed the first imaging results of a decimetric drifting structure (see Khan et al. 2002). The DPS patch was imaged with the NRH at 327 MHz (see Figure 6). It was accompanied by a soft X-ray plasmoid observed by *Yohkoh* SXT. Figure 6 indicates that the DPS radio source is located slightly above but overlapping with the plasmoid; however, the motion of the radio source was consistent with the plasmoid's motion.

The reported number of DPS events associated with plasmoid ejecta is small, and a meaningful statistical study is not yet available. Therefore, it is rather premature

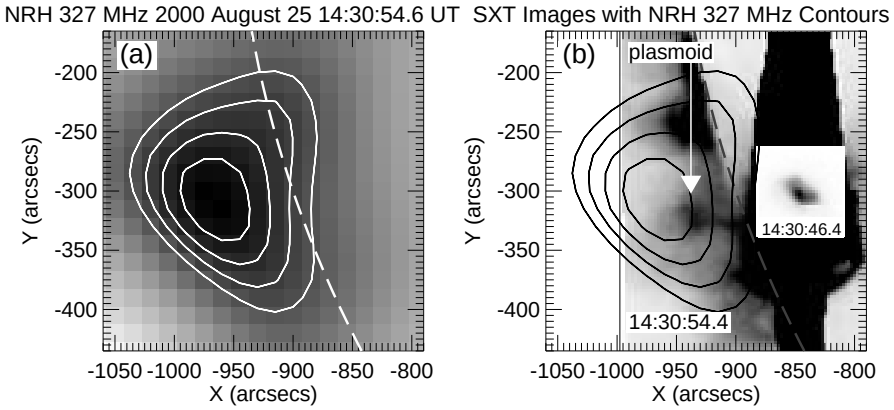

Fig. 6. Event of August 25, 2000 (from Khan et al. 2002). a) NRH 327 MHz source during the drifting continuum emission (which, unfortunatly, did not show clear pulsations at this frequency, see Fig. 1 of the original paper). b) The contours of a), now black, superposed on a composite SXT image. The radio source appears slightly ahead of the plasmoid.

to argue that DPS events are commonly associated with plasmoid ejections (or vice versa). But if future studies confirm this association, DPS events could provide diagnostics of the flare current sheet evolution, especially the plasma density near the acceleration site and the temporal characteristics of particle acceleration by magnetic reconnection.

4.2 Narrow-band Spikes

For decimetric spike bursts we refer to the review by Benz (1986). Individual spikes are very short (< 1 s), narrowband (some MHz only) bright emissions forming broadband clusters or patches of some tens to thousands during some tens of seconds to about a few minutes. Clusters are sometimes organized in small subgroups or chains. Sometimes they suggest quasi-periodic oscillatory temporal behavior at single-frequency records.

Using the spike's bandwidth, one may constrain its source size. If we assume that the emission frequency depends on a characteristic frequency (e.g. the local plasma frequency or a harmonic of the gyrofrequency) then an upper limit of spike's source dimension L is given by the product of the scale length of the characteristic frequency multiplied by $\Delta f/f$. Using typical values, Benz (1986) found than $L \leq 200$ km. Therefore, a successful model of narrowband spikes should be consistent with

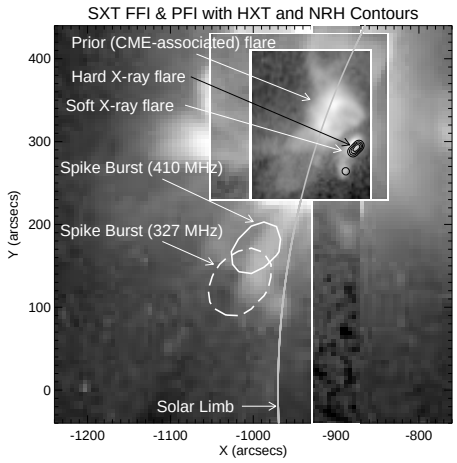

Fig. 7. Event of November 14, 1997. The gray-scale image is a composite of full-frame and partial frame *Yohkoh* SXT images. The black contours denote the hard X-ray image while white contours show the location of spike bursts according to Nançay maps (the solid contour corresponds to 410 MHz and the dashed contour to 327 MHz (Khan and Aurass, 2005).

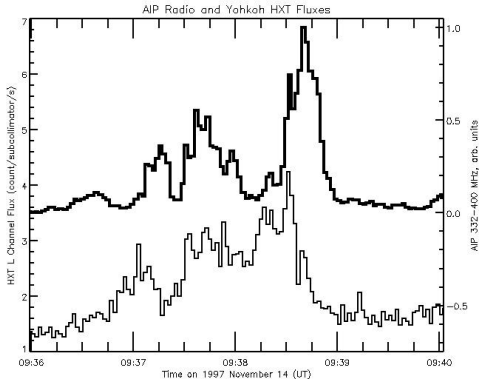

Fig. 8. Event of November 14, 1997. Frequency-integrated (332-400 MHz) radio spike flux taken from AIP spectral data (thick line), compared with *Yohkoh* HXR flux curve (14-23 keV) of the HXR source (Khan and Aurass, 2005).

very small source sizes. Traditionally, models considered the loss-cone instability of trapped electrons producing electron cyclotron maser emission at the footpoints of flaring loops (Melrose and Dulk 1982). To avoid high magnetic fields in the source region, the model has been modified to emission of upper-hybrid and Bernstein modes (Willes and Robinson 1996). This model can interpret the occasionally reported harmonic emission in decimetric spikes (Benz and Güdel 1987). Alternatively, Tajima et al. (1990) proposed that the spikes come from sources located in the acceleration site of the flare and result from waves produced by the acceleration process (see also Kuijpers et al. 1981; Stepanov et al. 1999).

In the working group sessions, particular attention was paid to whether or not decimetric spikes are signatures of accelerated particles at the primary energy release site. This type of radio emission has been traditionally interpreted as a signature of highly fragmented energy release in flares (Benz 1985). Barta and Karlický discussed their model (Barta and Karlický 2001) in which dm-spikes are generated in the turbulent plasma of reconnection outflows. According to this model, superthermal particles are accelerated near the X-point of the magnetic field, or directly in the cascading MHD turbulence, and lead to kinetic instabilities. Karlický argued that the presence of narrowband dm-spikes in the dynamic spectrum of the X1.5 flare of March 18, 2003 should be considered as a further argument supporting the reconnection scenario for that flare. In the same line of thought, Barta solved numerically a set of 2D MHD equations describing magnetic reconnection and determined the time evolution of the plasma parameters and magnetic field. From these results, he calculated the radio emission due to double resonance instability in reconnection jets. He showed that, depending on MHD turbulence properties, either "lace bursts" or dm-spikes should be observed ("lace bursts" is a rare type of fine structure observed in the 1-2 GHz frequency range which is characterized by rapid frequency variations, both positive and negative; see Jiřička et al. 2001).

However, contradictory results were also reported. Khan discussed a radio spike event observed with the Astrophysical Institute of Potsdam (AIP) spectrometer.

Using radio imaging data from the NRH and simultaneous soft and hard X-ray images from *Yohkoh* and EUV images from SOHO/EIT, he was able to determine the location of the spike bursts in relation to the flare and its environment. He found, as shown in Figure 7, that the location of the spike bursts was remote from the HXR source. Additionally, Figure 8 compares the (cluster-integrated) time profile of the radio flux of spike emission and the associated time profile of the hard X-ray emission. There is some correlation in the general behavior of the curves but not at all details. The movies presented by Khan indicated that the spike bursts occur at the site of compression of pre-existing loop structures. The compression was caused by a long-duration-event-associated CME which was launched nearby earlier (see also Fig. 7). The compression of the coronal loop structures can well result in magnetic reconnection leading to the spike burst event. Overall, the observations indicated that that particular spike burst event was merely a side-show to the main energy release which was associated with the CME/LDE event. The observations reported by Khan do not contradict earlier observations by Benz et al. (2002) who analyzed less convincing data suggesting that the spike clusters were located well outside the main energy release region of a flare.

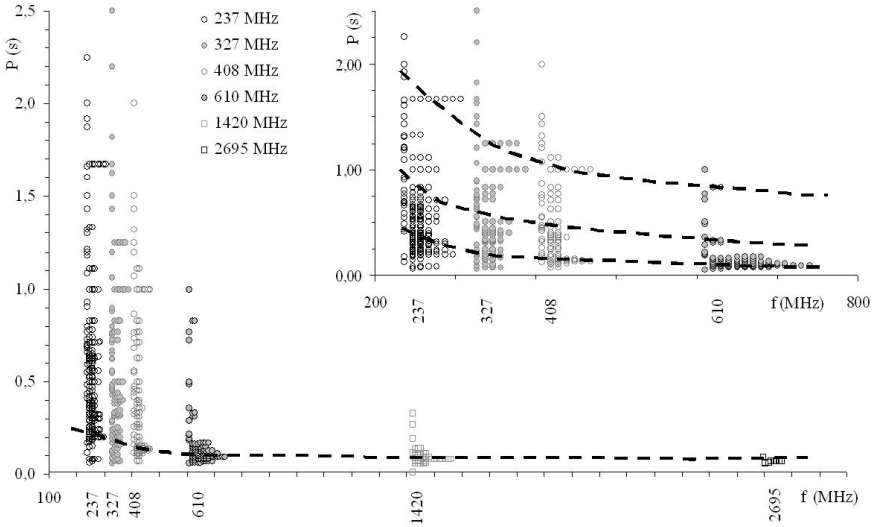

Fig. 9. Statistics of the dominant period of quasi-periodic fine structures in single-frequency Trieste Observatory polarimeter observations from January 1998 to July 2000 (courtesy of J. Magdalenič and P. Zlobec.)

5 Metric Pulsating Emission

5.1 Statistics

Magdalenič presented a statistical analysis of quasi-periodic oscillations selected from high time resolution single frequency records of Trieste Observatory (see also Magdalenić et al. 2002). Figure 9 gives "frequency-of-occurence" clusters over frequency for a 2.5-year sample (January 1998–June 2000). It is interesting that an $1/f$ dependence was found for the period range around 1 s. The high time resolution of Trieste single frequency records allowed Magdalenič to include shorter time scales in her study. It becomes clear that significant quasi-periodic flux fluctuations below 0.5 seconds occur over the whole spectral range, at least down to 200 MHz. If these very-short-period pulsations are due to MHD driver, then the Alfvén velocity can be used for a rough estimate of the typical source size (for the Trieste instrument's frequencies it lies between 500-1500 km s^{-1}; Vršnak et al. 2002). The resulting source dimensions corresponding to the very-short-period pulsations occurring at the low Trieste's frequencies are much smaller than the observed typical dimensions of coronal structures. Alternative mechanisms also need to be considered.

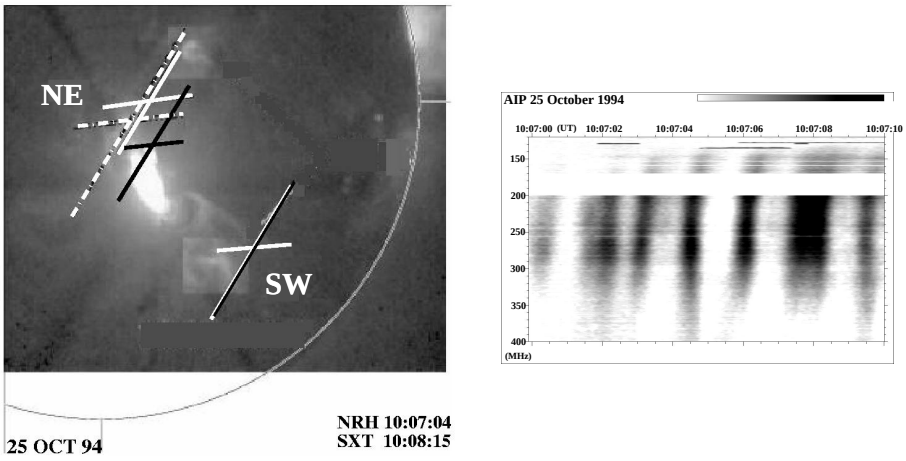

a) b)

Fig. 10. Meter-wave pulsation detail from Figure 1a. In a): single-pulse source configuration at 327 MHz. NE: main source site. Black cross: onset, white cross: end of the pulse. White-black stipple-dotted cross: source sites at 236.6 and 164 MHz. SW: secondary pulsation source site with 90 s lifetime. The sizes of the crosses give the half widths of the sources. The distance between the NE and SW source sites is $\approx$0.12 $R_\odot$. In b): the spectrum of this and neighboring pulses. Notice the J burst behavior at the low frequency edge.

5.2 Broad Band Pulsations

In the working group sessions, metric broad band pulsations (BBP) with non-drifting spectral envelopes were discussed by Aurass. He presented a BBP event with a complex source configuration that occured in a flaring sigmoidal loop system (Aurass et al. 2003). The analysis used radio spectral data from AIP while positional information was obtained from simultaneous NRH data. The pulsations' source sites were compared with soft X-ray images of the flare, and with force-free extrapolated coronal magnetic fields. Figure 10b shows an enlargement of the dynamic spectrum of the pulsations while in Figure 10a we present the source configuration at three different NRH frequencies superposed on a soft X-ray image of the flaring active region.

The BBP sources occur in a diverging loop-like structure with a turning height of about 70 Mm. A surprising result of Aurass's analysis was that for a time interval of 90 s during the main flare phase, individual pulses consist of one source at lower frequencies, but are formed by two simultaneous widely spaced sources at higher frequencies. These observations together with the event's magnetic field configuration suggest that the two high frequency sources must be fed by the same source of non-thermal electrons. This necessarily leads to the conclusion that in the given event, the broad band pulsations are due to a type III-like mechanism; the difference being in the source extent, and the density profile in the source. Furthermore, the beams exciting the pulse sequence are not accelerated within the radio-source-hosting configuration, but are injected near its strong-field footpoint. Note also that the double source of the pulsations was consistent with the overall evolution of the sigmoidal magnetic field configuration (see Aurass et al. 2003 for more details). It should be underlined here that in their pioneering work, Kai and Takayanagi (1973) came to the same conclusion concerning the beam-driven nature of broad band pulsations and the external beam injection site.

5.3 Zebra Patterns

Originally zebra patterns were explained in terms of the excitation of Bernstein modes at harmonics of the gyrofrequency in a quasi-homogeneous compact source (e.g. Rosenberg 1972). Another approach assumes that their origin is associated with enhanced generation of plasma waves in regions of inhomogeneous coronal loops where the condition of double plasma resonance $f_{\rm uh} = sf_{\rm B}$ is satisfied (e.g. Zheleznyakov and Zlotnik 1975, Kuijpers 1975, Winglee and Dulk 1986, Ledenev, Yan and Fu 2001). This means the local upper hybrid frequency must be equal to the harmonic number times the local gyrofrequency.

Referring to the inherent relation between the zebra pattern formation and broad band pulsations, Aurass described in the working group discussions the results of Aurass et al. (2003) and Zlotnik et al. (2003). Figure 11 gives the spectrum and positional data for a selected interval of the event shown in Figure 1a. They found a good correlation between the inclination of a single zebra stripe around 164 MHz and the projected speed derived from the motion of a radio source appearing in the 164 MHz NRH positional data.

Zlotnik et al. (2003) followed the double plasma resonance interpretation for the event they studied (according to Zheleznyakov & Zlotnik 1975, the Bernstein mode model cannot explain zebra patterns with more than 4-5 stripes). Their analysis

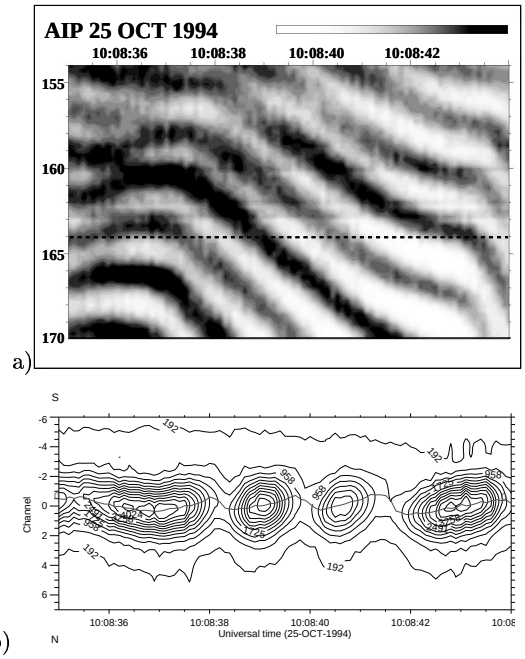

Fig. 11. Enlargement of the zebra pattern of Figure 1a. In a): spectrum (AIP). The stippled line denotes 164 MHz. In b): the NRH 164 MHz contours of equal brightness (North-South array). The vertical axis is graded in instrument-related units, corresponding to a field of 1.28 $R_\odot$. The dotted line gives the motion of the maximum of a Gaussian source model. Follow the stripes in the spectra and note the correlation of stripe inclination and source motion.

indicated that a grid of double resonance layers is formed along the weak field branch of the magnetically asymmetric source-carrying loop structure. A frequency drift of the stripe pattern results from the changes of the magnetic field or temperature in the source volume. Field decrease leads to an apparent motion of the source of a given stripe to regions of higher electron density. The source motion's speed in the radio images is proportional to the frequency drift rate of the stripes. In the same manner acts the effect of plasma cooling.

Zlotnik et al. (2003) tried to explain why sometimes (e.g. see our Figure 1a) in dynamic spectra we observe broad band pulsations first and then zebra stripes at lower frequencies: they argued that this is is due to the higher threshold of the double resonance instability compared to the beam instability.

5.4 Fiber Bursts

Fiber bursts are usually interpreted as the radio signature of whistler waves excited after their coalescence with Langmuir waves in loops with an unstable distribution of nonthermal electrons (Kuijpers 1975; Mann et al. 1987, 1989). An alternative approach has been followed by Bernold & Treumann (1983) and Treumann et al.

(1990) who invoked Alfvén solitons to explain fiber bursts. The two classes of models result in disturbances propagating either with the local whistler group velocity or with 1-3 times the local Alfvén velocity, respectively. Since at a given frequency, the modulator velocity is related to the burst's frequency drift rate, one can use the observed frequency drift rate to determine which model (if any) is more capable of explaining the observations.

Rausche presented observations of fiber bursts whose drift rates were consistent with the whistler wave model. He reported a promising new method that uses the drift rate and bandwidth measurements of fiber bursts as a probe of the magnetic field strength and 3D field structure in post-flare loops. The derived properties of the magnetic field can subsequently be compared directly with coronal magnetic field extrapolations. The method works when the fibers cross at least two frequencies for which positional information is available. It is based on the well-known property of whistler waves to propagate predominantly along magnetic field lines (e.g. Kuijpers 1975). Therefore, the radio source sites of fiber bursts at *two* frequencies determine (together with a coronal density model) a subset of field lines in the extrapolated coronal magnetic field. For more details on the method the reader is referred to the article by Aurass et al. (2005).

Rausche applied the method to the fiber bursts that occurred during the flare of April 7, 1997. Figure 12 summarizes the results. It shows the fiber burst-carrying field lines, forming an almost coplanar system during 1 hour of observations, overlaid

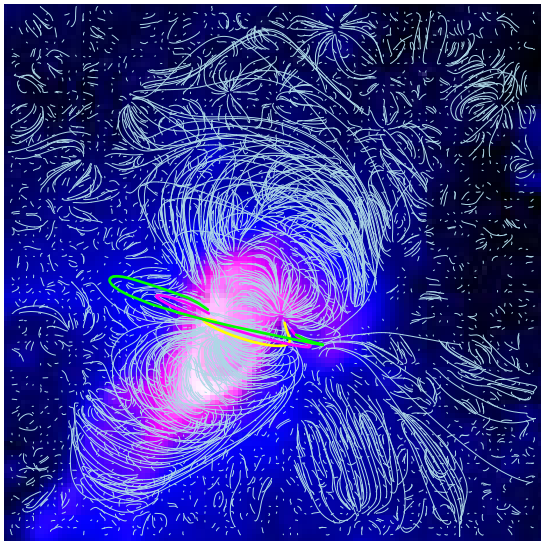

Fig. 12. *Yohkoh* postflare SXT image (07 April 1997, 16:40:28 UT, AlMg filter, 5.4 s exposure, N–upwards, W–to the right) with superposed potential field lines (white) and overplotted "mean fiber burst" field lines (Yellow line–10 min after impulsive phase, magenta–25 min after yellow, green–35 min after yellow). See also Aurass et al. (2005).

on a soft X-ray image. The figure also shows their location with respect to the full set of coronal field lines obtained from the potential field extrapolation of a SOHO/MDI magnetogram. Figure 13 quantitatively displays the evolution of the fiber-burst carrying post-flare loop field lines over the 1 hour time interval. It is surprising that the fiber bursts intermittently occur within the same height and magnetic field range despite the growth of the post-flare loop system. It is also interesting that the whistler waves driving the fiber emission are initially excited near the top of the post-flare loops, and later in the event almost at medium loop heights. Fig. 13 further reveals the extremely low field strength near the top of fiber-burst carrying post-flare loops 1 hour after the impulsive flare phase. From the footpoint locations of the field lines selected with the fiber burst data, a post-flare loop footpoint expansion speed can be estimated which is consistent with EUV and X-ray data.

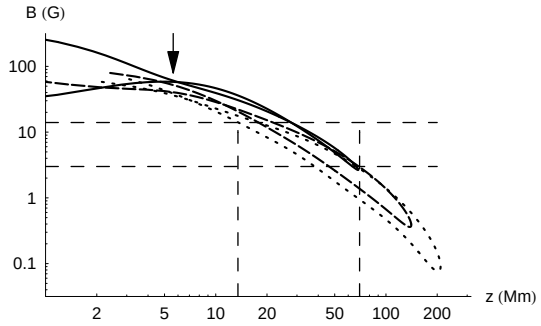

Fig. 13. Field strength versus height for the colored field lines in Figure 12. The solid, dashed and dotted curves correspond to the yellow, magenta, and green lines, respectively of Figure 12. All fiber bursts occur in the field strength–height range box formed by the long-dashed lines. The arrow points to a local field strength maximum occuring near the weak field end of the continuous line at height of about 5 Mm.

5.5 Source Model for Metric Fine Structure

It is well known (e.g. Slottje 1981) that broad band pulsations, fibers, and zebra patterns occur in complex radio bursts sometimes together (i.e. in the same flare event) and sometines not. On the other hand, not all flares with complex radio signatures show well-developed fine structures. With Figure 14 we outline the main properties of a source model for such fine structures following the results by Zlotnik et al. (2003).

What are the main features? All three types of fine structure occur in magnetically asymmetric loops (magnetic traps), at least at the beginning of fine structure emission during a given flare. The trap serves as the source of the accompanying

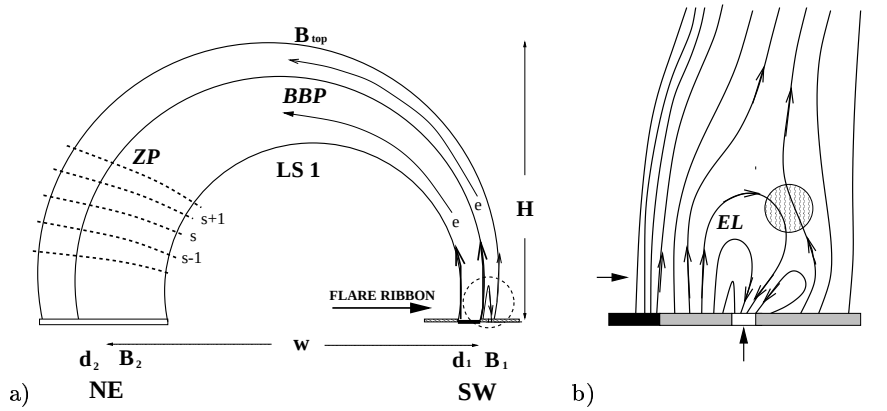

Fig. 14. Source model for metric continuum fine structures (Zlotnik et al. 2003). a) The loop LS1 is the main source of BBP and ZP (zebra patterns): fast electron streams exciting BBP are injected at the SW footpoint. ZP stripes arise at the double plasma resonance levels (stippled) in the NE part of LS1. b) Enlargement of the encircled SW region; the leading spot with polarity opposite to the polarity of the emerging loop (EL). The wavy circle is a site of reconnection and electron acceleration. This model refers to the analysis of the event shown in Figure 1a (see also Aurass et al. 2003).

broad band continuum emission by forming a loss-cone distribution of some background component of nonthermal electrons. Let us summarize some properties of the source model.

- A radio fine structure source needs nonthermal electrons. These seem to be injected during the associated flare mostly near the strong-field footpoint of the trap in the flaring active region. A possible source is the interaction between loops of different spatial scales as suggested e.g. by Hanaoka (1996) and Nishio et al (1997). Zaitsev et al. (2005) analyzed the efficiency of electron acceleration in such configuration.
- It is possible that the magnetic field near the strong-field footpoint interacts with part of a flaring structure (e.g. an approaching flare ribbon) and/or with emerging flux of parasitic polarity, possibly driving the loop interaction (with particle injection into the trap) into a periodic regime.
- Broad band pulsations seem to be due to repeated beam injection into the trap; this means metric pulsation pulses are type III-like emission within relatively small source structures. The radio source occurs between the strong-field footpoint and the top of the trap structure.
- Unlike pulsations, fibers and zebra stripe sources are located at the weak-field branch of the trap. Altynsev et al. (2005) analyzed microwave zebra stripes and came to the same conclusion at much higher frequencies.

- The analyzed events with meter-wave zebra stripes seem to support the models based on generation of electrostatic upper-hybrid waves at conditions of the double plasma resonance (e.g. Zheleznyakov & Zlotnik 1975, Zlotnik et al. 2003).
- For the analyzed events with decimeter/meter-wave fiber bursts, the Alfvén soliton fiber burst model of Treumann et al. (1990) can be ruled out. Fibers seem to be associated with whistler wave packets in coronal loops as proposed by Kuijpers (1975) and modified by Mann et al. (1987, 1989).

6 Summary and Future Work

In this section we present questions rather than conclusions. A firm conclusion, however, is that radio pulsations provide important diagnostics of the physical conditions in the corona. Most observations of radio pulsations come from non-imaging spectral data. The last few years, however, several studies that combine spectral data with simultaneous images obtained from the NoRH (microwaves) or NRH (decimetric-metric wavelengths) have appeared resulting in an accumulation of several well-observed events. These observations do not suffer from the positional ambiguities of earlier studies and have yielded significant progress in the subject. Furthermore, the combination of radio data with soft X-ray and EUV images from space telescopes offers the opportunity for a more complete view of the coronal configuration and the processes involved.

In comparing observations with theory, one has the feeling that the coupling between them has not reached the desired level yet. The observers often use formulas giving the periods of some MHD oscillation modes and compare them with their data. Of course, this is useful because it may provide diagnostics about the coronal plasma and magnetic field; however it does not tell much about the physical processes leading to radio emission modulation. On the other hand, theoretical studies need to take into account the latest observational results.

Clearly, we need to learn more about fundamendal processes leading to flares and coronal mass ejections. For example, can we use the "standard reconnection model" for the interpretation of dm drifting pulsating structures and spikes? In the working group sessions, such attempts were made, but only a couple of events were considered. In any case we cannot exclude other approaches. For instance, the appearance of decimetric spikes as evidence for the existence of multiple current sheets formed stochastically, versus evidence for spikes as a by-product of deterministic large-scale dynamic processes, needs to be tested. Furthermore, in the working group sessions, evidence for the beam-driven nature of broad band pulsations was presented for one event. A similar in-depth study needs to be done for several other BBP events before reaching firm conclusions.

In the working group sessions, several participants demonstrated how to exploit the information provided by radio pulsations in order to derive information about the coronal magnetic field. However, this process is not trivial and requires modeling at some stage. For example, the quasi-periodic fluctuations of strong steady sunspot-associated gyroresonance sources combined with models of the gyroresonance emission may yield accurate estimates about the underlying magnetic oscillations. Also, the combination of fiber burst data with magnetic field extrapolations provides a powerful tool to probe the 3D structure of post-flare loops.

Regarding microwave pulsations, an effort should be made to integrate the observations with longer wavelength radio, and coronal observations from space instruments. Observations of spatially resolved microwave oscillations (both from flares and the slowly-varying component) were presented in the meeting. This is a significant improvement but we believe that the use of simultaneous soft X-ray or/and EUV observations will provide additional progress. We do not know yet much about the relation between flare-related microwave oscillations and pulsations at metric wavelengths. In the study of decimetric and metric pulsations we need to clarify the associated magnetic field configuration. For example, in the working group sessions, there was a debate whether dm spike bursts are signatures of accelerated electrons at the primary energy release site or just a by-product of the main flare. Also, the possible association of dm drifting pulsating structures with plasmoid ejections needs to be tested with more observations. Here, the lack of simultaneous spectroscopic and imaging observations in the decimetric range is the main obstacle.

With the future development of the "Frequency Agile Solar Radiotelescope", imaging spectroscopy over a wide spectral range in radio will be achieved. This combined with the forthcoming space missions promises exciting new developments on the subject. Independently, broadband spectroscopy, possibly combined with extremely enhanced spectral and time resolution in subbands, will also remain a useful research tool in the future.

Acknowledgements

AN would like to thank Prof. C.E. Alissandrakis for useful discussions. He also acknowledges support from European Union's grant INTAS 00-543. HA acknowledges the European Office for Aerospace Research and Development for its support in maintaining the solar radio spectral observations at Potsdam.

References

1. A. Abrami: Solar Phys. **11**, 104 (1970)
2. A.T. Altyntsev, A.A. Kuznetsov, N.S. Meshalkina, Yihua Yan: Observations of zebra pattern in cm-range with spatial resolution, Adv. Space Res. accepted (2005)
3. A. Asai, M. Shimojo, H. Isobe, and 4 coauthors: ApJ **562**, L103 (2001)
4. M. Aschwanden: Solar Phys. **111**, 113 (1987)
5. M.J. Aschwanden, L. Fletcher, C.J. Schrijver, D. Alexander: ApJ **520**, 880 (1999)
6. M. Aschwanden, A.O. Benz: ApJ **332**, 447 (1988)
7. M. Aschwanden, V.M. Nakariakov, V.F. Melnikov: ApJ **600**, 458 (2004)
8. H. Aurass, K.-L. Klein, E. Ya. Zlotnik, V.V. Zaitsev: A&A **410**, 1001 (2003)
9. H. Aurass, G. Rausche, G. Mann, A. Hofmann: A&A **435**, 1137 (2005)
10. M. Barta, M. Karlický: A&A **379**, 1045 (2001)
11. L.R. Bellot-Rubio, M. Collados, B. Ruiz Cobo, I. Rodriguez Hidalgo: ApJ **534**, 989 (2000)
12. A.O. Benz: Solar Phys. **96**, 357 (1985)

13. A.O. Benz: Solar Phys. **104**, 99 (1986)
14. A.O. Benz, M. Güdel: Solar Phys. **111**, 175 (1987)
15. A.O. Benz, P. Saint-Hilaire, N. Vilmer: A&A **383**, 678 (2002)
16. N. Brynildsen, T. Leifsen, O. Kjeldseth-Moe, P, Maltby, K. Wilhelm: ApJ **511**, L121 (1999a)
17. N. Brynildsen, O. Kjeldseth-Moe, P, Maltby, K. Wilhelm:: ApJ **517**, L159 (1999b)
18. F. Dröge: A&A **57**, 285 (1977)
19. Ø. Elgarøy: *Solar Noise Storms* (Pergamon Oxford 1977), pp 177–185
20. G.D. Fleishman, Q.J. Fu, G.L. Huang, V.F. Melnikov, M. Wang: A&A **385**, 671 (2002)
21. A. Fludra: A&A **344**, L75 (1999)
22. G.B. Gelfreikh, V. Grechnev, T. Kosugi, K. Shibasaki: Solar Phys. **185**, 177 (1999)
23. N. Gopalswamy, E.J. Schmahl, M.R. Kundu: BAAS **25**, 1396 (1993)
24. V.V Grechnev, S.M. White, M.R. Kundu: ApJ **588**, 1163 (2003)
25. Y. Hanaoka: Double-Loop Configuration and Its Related Activities. In: *ASP Conf. Series* vol 111, ed. by R.D. Bentley, J.T. Mariska (Astron. Soc. of the Pacific, San Francisco 1996) pp 200–205
26. K. Hori: Study of Solar Decimetric Bursts with a Pair of Cutoff Frequencies. In: *Solar Physics with Radio Observations* NRO Report **479**, ed. by T. Bastian, N. Gopalswamy, K. Shibasaki (1999), pp 267–271
27. K. Jiřička, M. Karlický, H. Mészárosová, V. Snižek: A&A, **375**, 243 (2001)
28. K. Kai, A. Takayanagi: Solar Phys. **29**, 461 (1973)
29. M. Karlický: A&A **417**, 325 (2004)
30. M. Karlický, F. Fárník, and H. Mészárosová: A&A **395**, 677 (2002)
31. J.I. Khan, H. Aurass, H.: Observations of the Coronal Dynamics Associated with Solar Radio Spike Burst Emission, in preparation (2005)
32. J.I. Khan, N. Vilmer, P. Saint-Hilaire, A.O. Benz: A&A **388**, 363 (2002)
33. B. Kliem, M. Karlický, and A.O. Benz: A&A **360**, 715 (2000)
34. J. Kuijpers: Solar Phys. **44**, 173 (1975)
35. J. Kuijpers: Theory of Type IVdm Bursts. In: *Radiophysics of the Sun*, IAU Symp. **86** ed. by M. Kundu and T.E. Gergely (Reidel, Dordrecht 1980), pp 341–361
36. J. Kuijpers, P. van der Post, C. Slottje: A&A 103, 331 (1981)
37. V.G. Ledenev, Yi-Hua Yan, Qi-Jun Fu: Chin. Journ. of Astron. Astrophys **1**, 475 (2001)
38. B.W. Lites: Sunspot oscillations—Observations and implications. In: *Sunspots: Theory and observations; Proceedings of the NATO Advanced Research Workshop on the Theory of Sunspots* (Cambridge, United Kingdom, A93-47383 1992), p. 261-302
39. J. Magdalenić, P. Zlobec, M. Messerotti, B. Vrsnak: ESA SP-**506**, 335 (2002)
40. G. Mann, M. Karlický, U. Motschmann: Solar Phys. **110**, 381 (1987)
41. G. Mann, K. Baumgärtel, G.P. Chernov, M. Karlický: Solar Phys. **120**, 383 (1989)
42. D.J. McLean, K.V. Sheridan: Solar Phys. **32**, 485 (1973)
43. D.B. Melrose, G.A. Dulk: ApJ **259**, 844 (1982)
44. H. Nakajima: Solar Phys. **86**, 427 (1983)
45. V.M. Nakariakov, L. Ofman, E.E. Deluca, B. Roberts, J.M. Davila: Science **285**, Iss. 5429, 862 (1999)

46. V.M. Nakariakov, L. Ofman: A&A **372**, 53 (2001)
47. V.M. Nakariakov, A.V. Stepanov: this volume
48. V.M. Nakariakov, V.F. Melnikov, V.E. Reznikova: A&A **412**, L7 (2003)
49. A. Nindos, C.E. Alissandrakis, G.B. Gelfreikh, V.M. Bogod, C. Gontikakis: A&A **386**, 658 (2002)
50. M. Nishio, K. Yaji, T. Kosugi, H. Nakajima, T. Sakurai: ApJ, **489**, 976 (1997)
51. A. Norton, R.K. Ulrich, R.I. Bush, T.D. Tarbell: A&A 518, L123 (1999)
52. M. Ohyama, and K. Shibata: ApJ **499**, 934 (1998)
53. K. Yu. Platonov, G.D. Fleishman: Physics—Uspekhi **45** (3) 235 (2002)
54. Zhihai Qin, Chunseng Li, Qijun Fu, Zhengmin Gao: Solar Phys. **163**, 383 (1996)
55. B. Roberts, P.M. Edwin, A.O. Benz: Nature, **305**, 688 (1983)
56. B. Roberts, P.M. Edwin, A.O. Benz: ApJ **279**, 857 (1984)
57. H. Rosenberg: A&A **9**, 159 (1970)
58. H. Rosenberg: Sol. Phys., **25**, 188 (1972)
59. I. Rüedi, S.K. Solanki, J.O. Stenflo, T. Tarbell, P.H. Scherrer: A&A **335**, L97 (1998)
60. J.I. Sakai, C. de Jager: Space Sci. Rev. **77**, 1
61. K. Shibasaki: ApJ **550**, 326 (2001)
62. K. Shibata, and S. Tanuma: Earth Planets Space **53**, 473 (2001)
63. C. Slottje: *Atlas of Fine Structures of Dynamic Spectra of Solar Type IV-dm and Some Type II Radio Bursts* (Utrecht, Publ. Utrecht University 1981)
64. J. Staude: Sunspot Oscillations. In: *3rd Advances in Solar Physics Euroconference: Magnetic Fields and Oscillations*, ed. by B. Schmieder, A. Hofmann, J. Staude, (ASP Conf. Series 184, 1999), pp 113–123
65. A.V. Stepanov: Res. Geomagn., Aeronomy, and Solar Phys. (in Russ.) **54**, 141 (1980)
66. A.V. Stepanov, S. Urpo, V.V. Zaitsev: Solar Phys. **140**, 139 (1992)
67. A.V. Stepanov, B. Kliem, A. Krüger, J. Hildebrandt, V.I. Garaimov: ApJ **524**, 961 (1999)
68. T. Tajima, A.O. Benz, M. Thaker, J.N. Leboeuf: A&A **353**, 666 (1990)
69. S. Tanuma, T. Yokoyama, T. Kudoh, and K. Shibata: ApJ **551**, 312 (2001)
70. R.A. Treumann, M. Güdel, A.O. Benz: A&A **236**, 242 (1990)
71. G. Trottet, A. Kerdraon, A.O. Benz, R. Treumann: A&A **93**, 129
72. B. Vršnak, J. Magdalenić, H. Aurass, G. Mann: A&A, **396**, 673 (2002)
73. S.M. White, M.R. Kundu: Solar Phys. **174**, 31 (1997)
74. A.J. Willes, P.A. Robinson: ApJ **467**, 465 (1996)
75. R.M. Winglee, G.A. Dulk: ApJ **307**, 808 (1986)
76. C.W. Young, C.L. Spencer, G.E. Moreton: ApJ **133**, 243 (1961)
77. V.V Zaitsev: Solar Phys. **20**, 95 (1971)
78. V.V. Zaitsev, A.V. Stepanov: Soviet Astron. Letters **8**, 132 (1982)
79. V.V. Zaitsev, A.V. Stepanov: Soviet Astron. Letters **15**, 154 (1989)
80. V.V. Zaitsev, A.V. Stepanov, S. Urpo, S. Pohjolainen: A&A **337**, 887 (1998)
81. V.V. Zaitsev, E.Ya. Zlotnik, H. Aurass: *Astronomy Letters* **31**, 285 (2005)
82. V.V. Zheleznyakov, E.Ya. Zlotnik: Solar Phys. **43**, 431 (1975)
83. E. Ya. Zlotnik, V.V. Zaitsev, H. Aurass, G. Mann, A. Hofmann: Astron. Astrophys.**410**, 1011 (2003)